Chemical Engineering Journal 327 (2017) 336–342

Contents lists available at ScienceDirect

Chemical Engineering Journal

journal homepage: www.elsevier.com/locate/cej

Silver-decorated and palladium-coated copper-electroplated fibers derived from electrospun polymer nanofibers

Seongpil An [a,1], Yong Il Kim [a,1], Hong Seok Jo [a], Min-Woo Kim [a], Min Wook Lee [b,c], Alexander L. Yarin [a,b,*], Sam S. Yoon [a,*]

[a] School of Mechanical Engineering, Korea University, Seoul 02841, Republic of Korea
[b] Department of Mechanical and Industrial Engineering, University of Illinois at Chicago, 842 W. Taylor St., Chicago, IL 60607-7022, USA
[c] Multifunctional Structural Composite Research Center, Institute of Advanced Composites Materials, Korea Institute of Science and Technology, Chudong-ro 92, Bondong-eup, Wanju-gun, Jeollabuk-do 55324, Republic of Korea

HIGHLIGHTS

- Silver and palladium fibers were fabricated by the combination method.
- Fiber morphologies and elemental compositions were analyzed by SEM, EDX, and XPS.
- The high electrical performance of the fibers was exhibited with transparency.

ARTICLE INFO

Article history:
Received 22 February 2017
Received in revised form 8 June 2017
Accepted 15 June 2017
Available online 16 June 2017

Keywords:
Copper-electroplated fibers
Silver-decorated fibers
Palladium-coated fibers
Electrospinning
Electroplating
Ion-exchanging

ABSTRACT

Here we introduce novel methods of forming silver (Ag) and palladium (Pd) fibers. The Ag and Pd fibers are fabricated by the combination of electrospinning, electroplating, and ion-exchange techniques. Their properties are characterized by scanning electron microscope with energy dispersive X-ray spectroscopy, sheet resistance meter, UV–Vis spectrophotometer, and X-ray photoelectron spectroscope. These non-woven metal fibers are free-standing and film-shaped with high electrical conductivity, as well as flexibility. Such properties are attractive for future applications of these materials in various electrochemical processes.

1. Introduction

Various studies related to nano- and micro-fiber technologies have considerably contributed to technological advances at numerous fields of engineering [1] including batteries [2–6], solar cells [7,8], cooling high-power electronics [9–23], purification membranes [24], filters [25], drug delivery materials [26–31], self-healing composites [32–43], and so on. The growth of these fiber-related technologies is accordingly expected to increase continuously in the future. Among several fiber fabrication techniques [44–47], electrospun nanofibers have been most widely used for such high-tech engineering industries. Electrospinning is considered as one of the most effective methods of forming uniform nanofibers, which allows one to easily modify fiber diameters [48], to achieve a large surface area [49] and form fabrics of macroscopic sizes [50].

One of the most widely regarded advantages of using electrospun nanofibers is that it is possible to combine in them two or more materials, and/or combine electrospinning with the other fabrication processes. This enables formation of novel functionalized or uniquely structured nanofibers. For example, ceramic silica nanofibers were developed by mixing a polymer with other chemical materials [51], or silica-decorated carbon nanofibers were formed by using both electrospinning and dip coating [52]. More recently, high-performance transparent conducting electrodes (TCEs) were formed by using electrospinning and electroplating methods [53].

* Corresponding authors at: Department of Mechanical and Industrial Engineering, University of Illinois at Chicago, 842 W. Taylor St., Chicago, IL 60607-7022, USA (A.L. Yarin) and School of Mechanical Engineering, Korea University, Seoul 02841, Republic of Korea (S.S. Yoon).
E-mail addresses: ayarin@uic.edu (A.L. Yarin), skyoon@korea.ac.kr (S.S. Yoon).
[1] These authors contributed equally to this work.

http://dx.doi.org/10.1016/j.cej.2017.06.076
1385-8947/

Copper (Cu) and silver (Ag) belong to the group of the most extensively studied metals for electrochemical applications due to their superior electrical conductivity, non-toxicity, and easy availability [54,55]. In particular, they have revealed enhanced performances when fabricated with nano- or micro-sized dimensions such as in Cu- and Ag-nanowires. Palladium (Pd) has been also broadly used as a catalyst in various fields [56,57]. However, the use of these metals in nano-scale objects has been continuously challenged because of complex fabrication processes and scalability problems.

Here, we introduce a novel method of fabrication of Ag-decorated and Pd-coated fibers by combining electrospinning, electroplating, and ion-exchange methods. The Ag-decorated fibers are core-shell structured with Cu, and thus possess not only highly textured surfaces but also superior electrical conductivities. The intact Pd-covered nanofibers are introduced for the first time. These fibers are attractive as a novel catalytic chemical material.

2. Experimental methods

2.1. Materials

Polyacrylonitrile (PAN, M_w = 150 kDa) and *N,N*-dimethylformamide (DMF, 99.8%) for a solute and a solvent, respectively, were purchased from Sigma-Aldrich. The 8 wt% PAN solution was prepared by dissolving PAN powder in DMF and magnetically stirred until becoming homogeneous. Sulfuric acid (H_2SO_4, >97.5%), hydrochloric acid (HCl, >35%), copper (II) sulfate ($CuSO_4$, >99.99%), and formaldehyde (>35%) were also purchased from Sigma-Aldrich and mixed at the fixed ratio for the electroplating solution (Table 1). Silver nitrate ($AgNO_3$, >99.0%) was also purchased from Sigma-Aldrich, and 0.01, 0.03, and 0.06 wt% of $AgNO_3$ powder were dissolved in DI water and magnetically stirred until becoming homogenous to prepare the ion-exchanging solution. Palladium (II) nitrate ($Pd(NO_3)_2$) hydrate was also obtained from Sigma-Aldrich, and 1 wt% $Pd(NO_3)_2$ hydrate powder was dissolved in DI water and stirred similarly to the $AgNO_3$ solution.

2.2. Copper-electroplating of electrospun polyacrylonitrile nanofibers

Silver (Ag) and palladium (Pd) were deposited by ion-exchange onto copper (Cu)-electroplated fibers. The Cu-electroplated fibers were fabricated using a recently introduced method where metals were electroplated onto electrospun polymer nanofibers [10,53]. It should be emphasized that Cu-electroplated fibers could acquire different chemical compositions (either being pure Cu or Cu_xO) with the drying atmosphere being either an inert gas or air, respectively. Fig. 1 illustrates how the fiber morphology and structure change according to the fabrication process used. First, PAN nanofibers were electrospun onto a Cu-frame under the fixed conditions listed in Table 2 and depicted in Fig. 1a. Then, platinum (Pt) was sputtered with a thickness of a few nm (not shown here) to impart a minimum conductivity for the following electroplating process. Next, the Cu-frame with the deposited nanofibers (cathode) was electroplated using a thin Cu-film (anode) at the fixed conditions (Table 3) and then dried in an inert gas atmosphere. Drying in the inert gas prevented oxidation of the Cu-electroplated fibers, thus, pure Cu-fibers were obtained as illustrated in Fig. 1b.

2.3. Silver ion-exchange on copper-electroplated fibers

Prior to the ion-exchange process, the free-standing Cu-electroplated fibers (which were suspended on the Cu-frame, cf. Section 2.2) were transferred onto supporting glass slides, which prevented the Cu-electroplated fibers from being floated in the

Table 1
Electroplating solution. Each 'weight ratio' value is based on the hydrochloric acid weight as 1.

Material	Weight ratio
Sulfuric acid	10
Hydrochloric acid	1
Copper sulfate	32
Formaldehyde	20
DI water	200

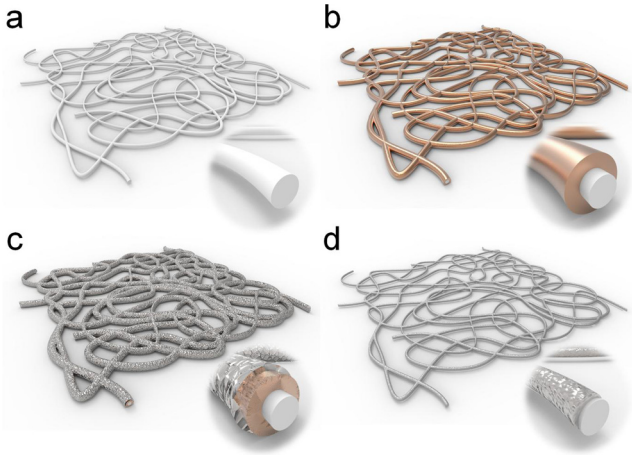

Fig. 1. Schematic of: (a) the electrospun PAN nanofibers, (b) the Cu-electroplated fibers, (c) the Ag-decorated fibers formed by ion-exchange, and (d) the Pd-coated fibers formed by ion-exchange.

Table 2
Experimental conditions for electrospinning PAN nanofibers.

Parameter	Value
Flow rate (μL/h)	200
Applied voltage (V)	8
Needle size	18-gauge
Needle-to-substrate distance (cm)	15
Electrospinning time (s)	90

Table 3
Experimental conditions for electroplating the PAN nanofibers.

Parameter	Value
Applied voltage (V)	3
Electrode size (cm^2)	3.5 × 2.5
Cathode-to-anode distance (cm)	2
Electroplating time (s)	7

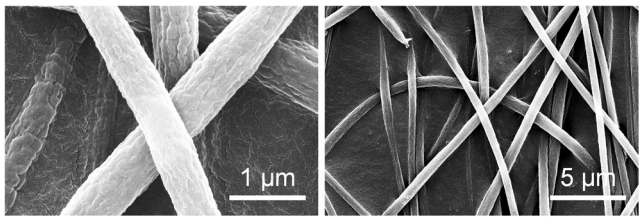

Fig. 2. SEM images of the electrospun PAN nanofibers.

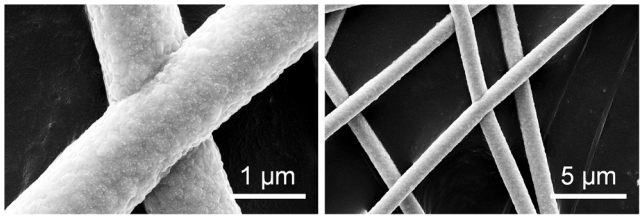

Fig. 3. SEM images of the Cu-electroplated fibers.

ion-exchange solution. The Cu-electroplated fibers on a slide glass were immersed into the $AgNO_3$ solution (cf. Section 2.1) for tens of minutes, and then, silver (Ag)-decorated fibers were obtained as illustrated in Fig. 1c.

2.4. Palladium ion-exchange on copper-electroplated fibers

The Cu-electroplated fibers on a slide glass (cf. Section 2.3) were immersed into the $Pd(NO_3)_2$ hydrate solution (cf. Section 2.1) for tens of minutes, and then, the intact palladium (Pd)-covered fibers were obtained as depicted in Fig. 1d.

2.5. Characterization

Fiber morphologies and elemental compositions were characterized by a field-emission scanning electron microscope with energy dispersive X-ray spectroscopy (FE-SEM/EDX, Quanta 250 FEG, FEI). Samples for SEM were prepared by taping fibers (on a slide glass) with a carbon tape and sputtering Pt to facilitated clear images. Note that few fibers were buried in the carbon tape in the

Table 4
Sheet resistances of fiber mats of different types. Each 'ρ ratio' value is based on the electrical resistivity of Cu-electroplated fibers taken as 1.

Fiber type	Ion-exchange solution concentration (C_{ex}, wt%)	Ion-exchange time (t_{ex}, min)	Sheet resistance (R_s, Ω/sq)	R_s ratio	Electrical resistivity of bulk at 20 °C [67] (ρ, Ω·m)	ρ ratio
PAN	–	–	∞	∞	∞	∞
Cu-electroplated	–	–	0.206	1	1.68×10^{-8}	1
Ag-decorated	0.01	60	0.298	1.4	1.59×10^{-8}	0.9
		90	0.225	1.1		
		120	0.264	1.3		
	0.03	60	0.394	1.9		
	0.06	60	2.21	11		
Pd-coated	1	90	472	2293	1.05×10^{-7}	6.3
		180	324	1575		
		270	513	2493		

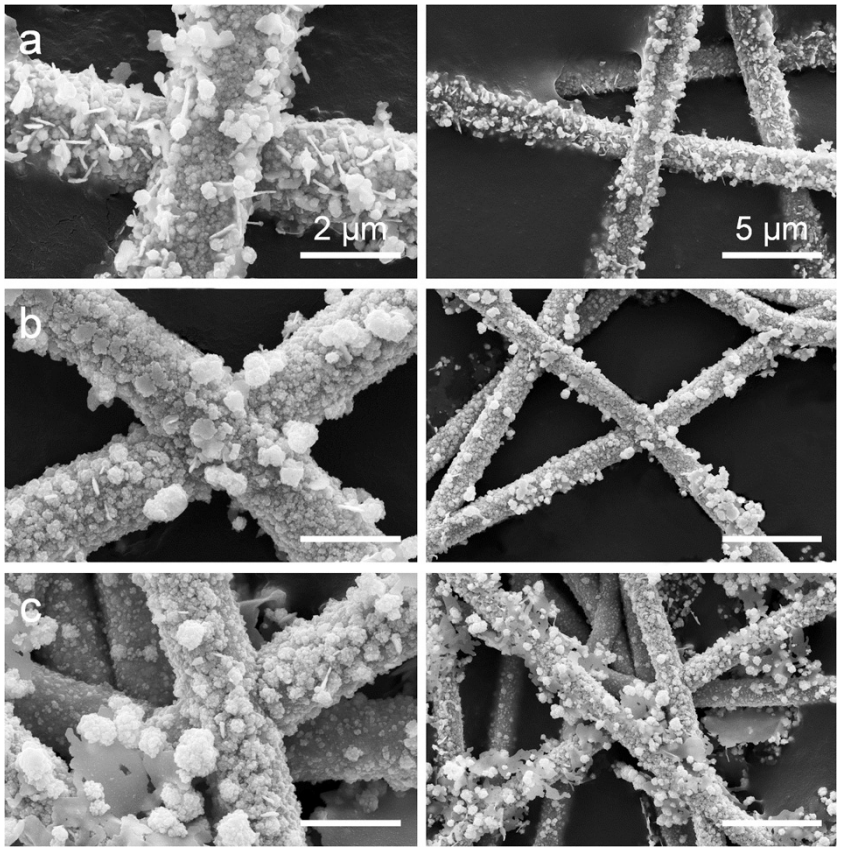

Fig. 4. SEM images of the Ag-decorated fibers as a function of time t_{ex} with the fixed value of C_{ex} of 0.01 wt%: (a) t_{ex} = 60 min, (b) t_{ex} = 90 min, and (c) t_{ex} = 120 min.

process of transferring a sample onto the tape (cf. Fig. 2). The fiber-size distribution was evaluated by measuring 100 nanofibers in SEM images. The transmittances of free-standing fiber mats were in the 50 to 60% range. They were measured by a UV–Vis spectrophotometer (Optizen POP, Mecasys). Sheet resistance values were obtained by averaging 10 values at different locations of each sample on a glass slide using a sheet resistance meter (FPP-400, Dasol Eng). Qualitative analyses were conducted by using X-ray photoelectron spectroscope (XPS, X-tool, ULVAC-PHI).

3. Results and discussion

3.1. Copper-electroplated fibers

Fig. 2 shows SEM images of electrospun PAN nanofibers. The average diameter (D_{avg}) of these nanofibers was 550 ± 67 nm. After Cu-electroplating and drying in nitrogen, the value of D_{avg} was increased to 1111 ± 87 nm and pure Cu-fibers with smooth surface were obtained as shown in Fig. 3. It should be emphasized that fiber junctions between two or more fibers (cf. Fig. 2) were fused in the electroplating process as observed in Fig. 3. This enabled the overall electrical conductivity of the fiber layer to be significantly increased due to the reduced contact resistance at the junctions [53]. Accordingly, the sheet resistance (R_s) of the Cu-electroplated fibers was remarkably low, namely 0.206 Ω/sq (Table 4), which is a great advantage for various transparent conducting electrode (TCE) applications, including touch screens [58], displays [59], light emitting diodes (LEDs) [60], and so on. Note that the diameter of the Cu-electroplated fibers can be varied in the hundreds of nm to a few μm range by varying the experimental conditions (not shown here, cf. Table 3).

3.2. Silver-decorated fibers

Fig. 4 shows SEM images of Ag-decorated fibers with varying the ion-exchange time (t_{ex}) at a fixed solution concentration (C_{ex}). The Cu-fiber surface was gradually decorated by granular-like Ag as t_{ex} increased. While the outermost Cu on the fiber surface was ion-exchanged, the overall Cu on the fibers was not totally replaced by Ag; see Figs. 4 and 5. This resulted in an increase of the fiber diameter D_{avg} (i.e., D_{avg} = 1402 ± 85 nm for t_{ex} = 90 min)

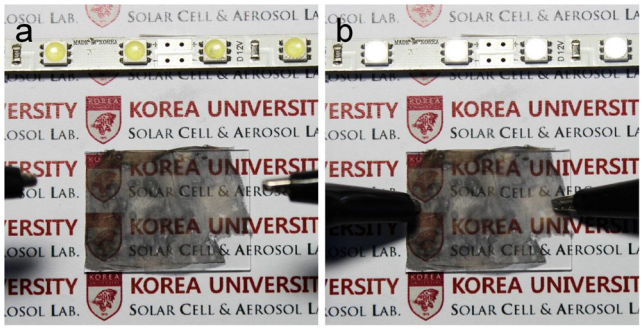

Fig. 6. Photographs of the Ag-decorated fiber layer transferred onto a glass slide. The value of C_{ex} = 0.01 wt%, and t_{ex} = 90 min. (a) Before, and (b) after LED operation.

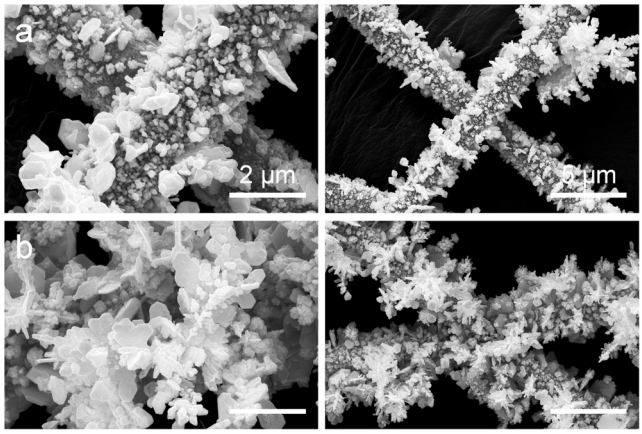

Fig. 7. SEM images of the Ag-decorated fibers as a function of the concentration C_{ex} at the fixed t_{ex} = 60 min: (a) C_{ex} = 0.03 wt%, and (b) C_{ex} = 0.06 wt%.

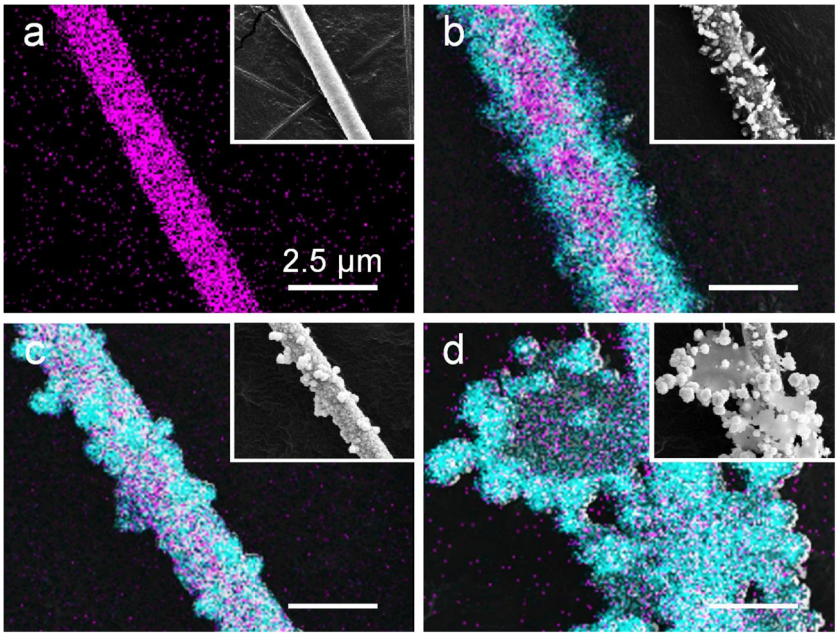

Fig. 5. Elemental mapping SEM images of the Ag-decorated fibers as a function of time t_{ex} with the fixed value of C_{ex} of 0.01 wt%: (a) t_{ex} = 0 (or pure Cu-electroplated fiber), (b) t_{ex} = 60 min, (c) t_{ex} = 90 min, and (d) t_{ex} = 120 min (Purple: Cu and sky-blue: Ag). (For interpretation of the references to colour in this figure legend, the reader is referred to the web version of this article.)

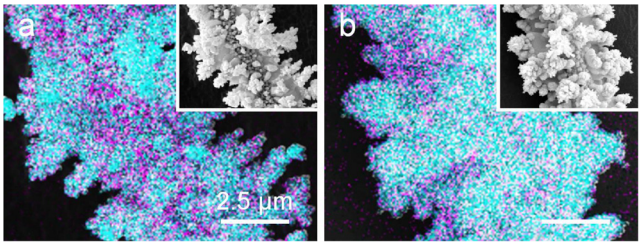

Fig. 8. Elemental mapping SEM images of the Ag-decorated fibers as a function of the concentration C_{ex} at the fixed t_{ex} = 60 min: (a) C_{ex} = 0.03 wt% and (b) C_{ex} = 0.06 - wt% (Purple: Cu and sky-blue: Ag). (For interpretation of the references to colour in this figure legend, the reader is referred to the web version of this article.)

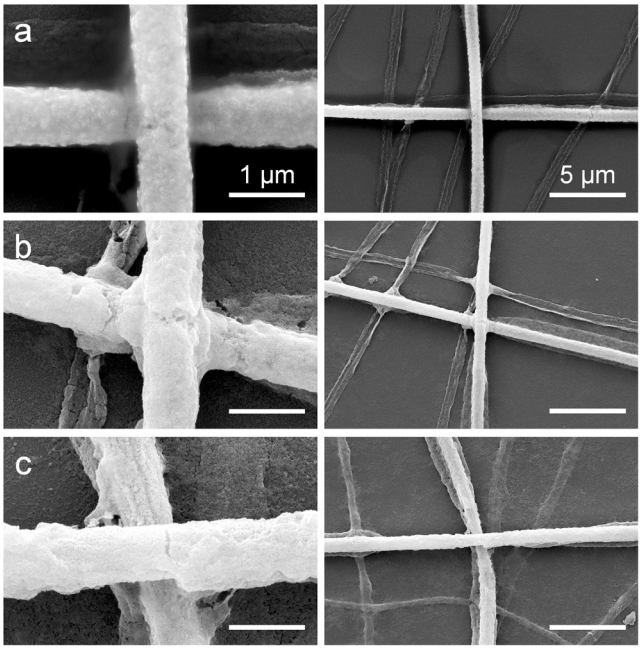

Fig. 9. SEM images of the Pd-coated fibers as a function of t_{ex} at the fixed C_{ex} of 1 wt %: (a) t_{ex} = 90 min, (b) t_{ex} = 180 min, and (c) t_{ex} = 270 min.

compared to that of the Cu-electroplated fibers (cf. Section 3.1). Both the increased fiber diameter and the textured rough surface cause R_s to increase by a factor of 1.1, 1.3, and 1.4 as listed in Table 4. Note that the smoothest surface case (t_{ex} = 90 min, cf. Fig. 4b) revealed the smallest change in R_s by a factor of 1.1. Such novel highly conductive (Table 4, Figs. 6 and S1) Cu/Ag core-shell fiber mats (in fact, triple-layered, with PAN at the center as illustrated in Fig. 1c) with an increased surface area hold great promise in various electrochemical applications. Indeed, Cu_2O/Ag [61,62] or CuO/Ag [63–66] core-shell fibers could be also obtained by changing a drying atmosphere from the inert gas to air (cf. Section 2.2) as demonstrated in detail in Supporting Information Figs. S2 and S3.

Figs. 7 and 8 show changes in the morphology and elemental composition, respectively, when varying C_{ex} from 0.03 to 0.06 wt % at the fixed t_{ex} = 60 min. While all the cases with C_{ex} = 0.01 wt% revealed the low-height granular-like growths on the fiber surfaces (cf. Fig. 4) regardless of t_{ex}, varying of C_{ex} resulted in the high-height fractal-like growths on the surfaces as C_{ex} increased. Note in addition, that the R_s increased by a factor of 1.9 and 11 compared to the Cu-electroplated fibers, which was also caused by the increased fiber diameter and the roughened surface.

3.3. Palladium-coated fibers

Contrary to the Ag-decorated fibers, the Pd-coated fibers revealed full coverage of the surface by Pd without visible traces of Cu, in distinction from Ref. [1], as shown in Figs. 9 and 10. Note that the Pd ion-exchange was not well-performed below C_{ex} = 1 wt % (not shown here). For this reason, the Pd ion-exchange was conducted at the fixed C_{ex} = 1 wt% with varying t_{ex} from 90 to 270 min. There was no discernible change in the fiber diameter D_{avg} at increasing t_{ex} (Fig. 9). However, it should be emphasized that the amount of Pd on the fiber surface gradually increased (Fig. 10). Note that a small fraction of Cu in Fig. 10 was found by a sampling process described in Section 2.5. It seems that the R_s values were significantly increased comparing to the Cu-electroplated fibers (Table 4). The listed value of R_s stems from a decreased fiber diameter and an increased contact resistance.

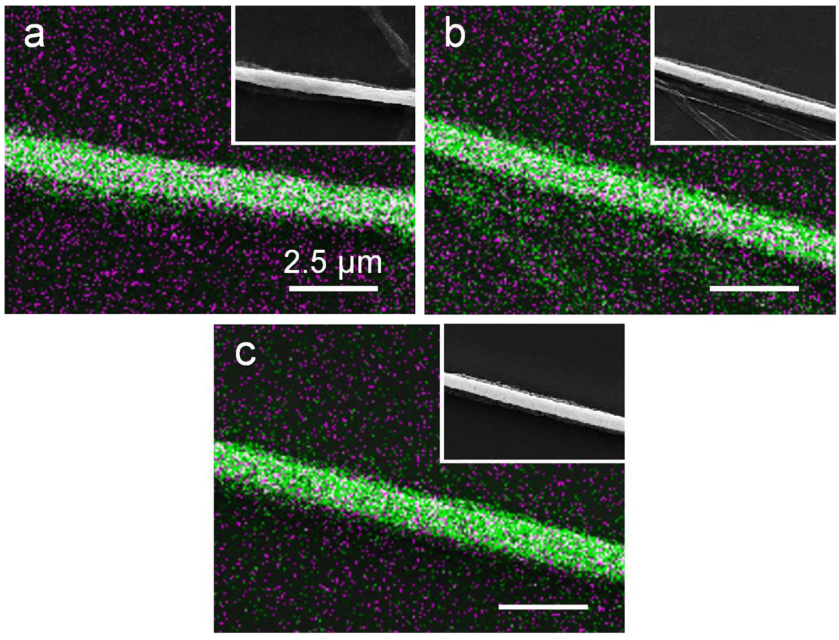

Fig. 10. Elemental mapping SEM images of the Pd-coated fibers as a function of time t_{ex} at the fixed C_{ex} of 1 wt%: (a) t_{ex} = 90 min, (b) t_{ex} = 180 min, and (c) t_{ex} = 270 min (Purple: Cu and green: Pd). (For interpretation of the references to colour in this figure legend, the reader is referred to the web version of this article.)

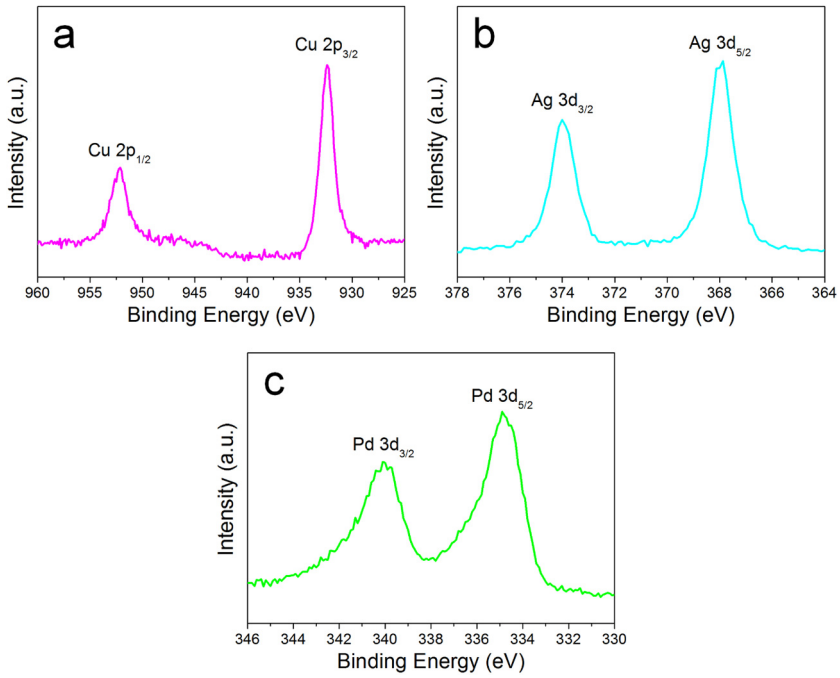

Fig. 11. High-resolution XPS spectra for different fiber types: (a) Cu 2p of the Cu-electroplated fibers, (b) Ag 3d of the Ag-decorated fibers for C_{ex} = 0.01 wt% and t_{ex} = 120 min, and (c) Pd 3d of the Pd-coated fibers for t_{ex} = 180 min.

3.4. XPS analysis

To characterize the fibers qualitatively, XPS analyses were conducted as shown in Fig. 11 and Supporting Information Fig. S4. Note that the C 1s peak of 284 eV was used as the reference for calibration. Fig. 11 shows the high-resolution Cu 2p, Ag 3d, and Pd 3d XPS spectra of the Cu-electroplated, the Ag-decorated, and the Pd-coated fibers, respectively. First, the two main peaks in Fig. 11a are located at 953 and 933 eV, which corresponds to Cu $2p_{1/2}$ and Cu $2p_{3/2}$, respectively. Next, the two main peaks located at 374 and 368 eV in Fig. 11b are assigned to Ag $3d_{3/2}$ and Ag $3d_{5/2}$, respectively. Third, the two main peaks at 340 and 335 eV in Fig. 11c correspond to Pd $3d_{3/2}$ and Pd $3d_{5/2}$, respectively. These XPS results indicate the presence of Cu, Ag, and Pd in the fabricated fibers. Note that the existence of Si and O in the XPS full spectra (Supporting Information Fig. S4) was derived from the slide glass (cf. Section 2) mainly composed of amorphous SiO_2.

4. Conclusion

We have demonstrated newly introduced approaches developed to form silver (Ag)-decorated and palladium (Pd)-coated fibers via an ion-exchange method applied to copper (Cu)-electroplated fibers. The Cu-electroplated fibers were obtained by electrospinning followed by electroplating. The Ag and Pd ion-exchanges were conducted by immersing the Cu-electroplated fibers in silver nitrate ($AgNO_3$) and palladium (II) nitrate ($Pd(NO_3)_2$) hydrate olutions, respectively. The Ag-decorated fibers were not only core-shell structured but also nano-textured with an excellent sheet resistance values ranging from 0.225 to 2.21 Ω/sq. In addition, the nano-scaled Pd-coated fibers were successfully obtained with reasonable sheet resistance values, which is the reported for the first time for Pd nanofibers. The fabricated metal fibers herein hold great promise for improving electrochemical performance in various engineering fields, including photoelectrochemical (PEC) water splitting devices, solar cells, batteries, supercapacitors, and transparent conducting electrodes.

Acknowledgements

This research was supported by the Technology Development Program to Solve Climate Changes of the National Research Foundation (NRF) funded by the Ministry of Science, ICT & Future Planning (2016M1A2A2936760), NRF-2013M3A6B1078879, and NRF-2017R1A2B4005639.

Appendix A. Supplementary data

Supplementary data associated with this article can be found, in the online version, at http://dx.doi.org/10.1016/j.cej.2017.06.076.

References

[1] A.L. Yarin, B. Pourdeyhimi, S. Ramakrishna, Fundamentals and Applications of Micro-and Nanofibers, Cambridge University Press, Cambridge, 2014.
[2] S. Chen, H. Hou, F. Harnisch, S.A. Patil, A.A. Carmona-Martinez, S. Agarwal, Y. Zhang, S. Sinha-Ray, A.L. Yarin, A. Greiner, Electrospun and solution blown three-dimensional carbon fiber nonwovens for application as electrodes in microbial fuel cells, Energy Environ. Sci. 4 (2011) 1417–1421.
[3] L. Dimesso, C. Spanheimer, W. Jaegermann, Y. Zhang, A.L. Yarin, $LiFePO_4$–3D carbon nanofiber composites as cathode materials for Li-ions batteries, J. Appl. Phys. 111 (2012) 064307.
[4] H. Wu, G. Chan, J.W. Choi, Y. Yao, M.T. McDowell, S.W. Lee, A. Jackson, Y. Yang, L. Hu, Y. Cui, Stable cycling of double-walled silicon nanotube nattery anodes through solid-electrolyte interphase control, Nat. Nanotechnol. 7 (2012) 310–315.
[5] L. Dimesso, C. Spanheimer, W. Jaegermann, Y. Zhang, A.L. Yarin, $LiCoPO_4$—3D carbon nanofiber composites as possible cathode materials for high voltage applications, Electrochim. Acta 95 (2013) 38–42.
[6] J. Hao, G. Lei, Z. Li, L. Wu, Q. Xiao, L. Wang, A novel polyethylene terephthalate nonwoven separator based on electrospinning technique for lithium ion battery, J. Membr. Sci. 428 (2013) 11–16.
[7] P. Joshi, L. Zhang, Q. Chen, D. Galipeau, H. Fong, Q. Qiao, Electrospun carbon nanofibers as low-cost counter electrode for dye-sensitized solar cells, ACS Appl. Mater. Interfaces 2 (2010) 3572–3577.
[8] S. Dharani, H.K. Mulmudi, N. Yantara, P.T.T. Trang, N.G. Park, M. Graetzel, S. Mhaisalkar, N. Mathews, P.P. Boix, High efficiency electrospun TiO_2 nanofiber based hybrid organic–inorganic perovskite solar cell, Nanoscale 6 (2014) 1675–1679.
[9] R. Srikar, T. Gambaryan-Roisman, C. Steffes, P. Stephan, C. Tropea, A.L. Yarin, Nanofiber coating of surfaces for intensification of drop or spray impact cooling, Int. J. Heat Mass Transfer 52 (2009) 5814–5826.

[10] S. Sinha-Ray, Y. Zhang, A.L. Yarin, Thorny devil nanotextured fibers: the way to cooling rates on the order of 1 kW/cm^2, Langmuir 27 (2010) 215–226.
[11] C.M. Weickgenannt, Y. Zhang, A.N. Lembach, I.V. Roisman, T. Gambaryan-Roisman, A.L. Yarin, C. Tropea, Nonisothermal drop impact and evaporation on polymer nanofiber mats, Phys. Rev. E 83 (2011) 036305.
[12] C.M. Weickgenannt, Y. Zhang, S. Sinha-Ray, I.V. Roisman, T. Gambaryan-Roisman, C. Tropea, A.L. Yarin, Inverse-Leidenfrost phenomenon on nanofiber mats on hot surfaces, Phys. Rev. E 84 (2011) 036310.
[13] S. Jun, S. Sinha-Ray, A.L. Yarin, Pool boiling on nano-textured surfaces, Int. J. Heat Mass Transfer 62 (2013) 99–111.
[14] S. An, C. Lee, M. Liou, H.S. Jo, J.-J. Park, A.L. Yarin, S.S. Yoon, Supersonically blown ultrathin thorny devil nanofibers for efficient air cooling, ACS Appl. Mater. Interfaces 6 (2014) 13657–13666.
[15] S. Sinha-Ray, A.L. Yarin, Drop impact cooling enhancement on nano-textured surfaces. Part I: Theory and results of the ground (1g) experiments, Int. J. Heat Mass Transfer 70 (2014) 1095–1106.
[16] S. Sinha-Ray, S. Sinha-Ray, A.L. Yarin, C.M. Weickgenannt, J. Emmert, C. Tropea, Drop impact cooling enhancement on nano-textured surfaces. Part II: results of the parabolic flight experiments [zero gravity (0g) and supergravity (1.8 g)], Int. J. Heat Mass Transfer 70 (2014) 1107–1114.
[17] R.P. Sahu, S. Sinha-Ray, S. Sinha-Ray, A.L. Yarin, Pool boiling on nano-textured surfaces comprised of electrically-assisted supersonically solution-blown, copper-plated nanofibers: experiments and theory, Int. J. Heat Mass Transfer 87 (2015) 521–535.
[18] R.P. Sahu, S. Sinha-Ray, S. Sinha-Ray, A.L. Yarin, Pool boiling of Novec 7300 and self-rewetting fluids on electrically-assisted supersonically solution-blown, copper-plated nanofibers, Int. J. Heat Mass Transfer 95 (2016) 83–93.
[19] S. Sinha-Ray, W. Zhang, R.P. Sahu, S. Sinha-Ray, A.L. Yarin, Pool boiling of Novec 7300 and DI water on nano-textured heater covered with supersonically-blown or electrospun polymer nanofibers, Int. J. Heat Mass Transfer 106 (2016) 482–490.
[20] V.K. Patel, J. Seyed-Yagoobi, S. Sinha-Ray, S. Sinha-Ray, A. Yarin, Electrohydrodynamic conduction pumping-driven liquid film flow boiling on bare and nanofiber-enhanced surfaces, J. Heat Transfer 138 (2016) 041501.
[21] M. Freystein, F. Kolberg, L. Spiegel, S. Sinha-Ray, R.P. Sahu, A.L. Yarin, T. Gambaryan-Roisman, P. Stephan, Trains of Taylor bubbles over hot nano-textured mini-channel surface, Int. J. Heat Mass Transfer 93 (2016) 827–833.
[22] S. An, H.S. Jo, S.S. Al-Deyab, A.L. Yarin, S.S. Yoon, Nano-textured copper oxide nanofibers for efficient air cooling, J. Appl. Phys. 119 (2016) 065306.
[23] H. Yoon, M.-W. Kim, H. Kim, D.-Y. Kim, S. An, J.-G. Lee, B.N. Joshi, H.S. Jo, J. Choi, S.S. Al-Deyab, Efficient heat removal via thorny devil nanofiber, silver nanowire, and graphene nanotextured surfaces, Int. J. Heat Mass Transfer 101 (2016) 198–204.
[24] M.W. Lee, S. An, S.S. Latthe, C. Lee, S. Hong, S.S. Yoon, Electrospun polystyrene nanofiber membrane with superhydrophobicity and superoleophilicity for selective separation of water and low viscous oil, ACS Appl. Mater. Interfaces 5 (2013) 10597–10604.
[25] S. Sinha-Ray, S. Sinha-Ray, A.L. Yarin, B. Pourdeyhimi, Application of solution-blown 20–50 nm nanofibers in filtration of nanoparticles: the efficient van der Waals collectors, J. Membr. Sci. 485 (2015) 132–150.
[26] J.K. Wise, A.L. Yarin, C.M. Megaridis, M. Cho, Chondrogenic differentiation of human mesenchymal stem cells on oriented nanofibrous scaffolds: engineering the superficial zone of articular cartilage, Tissue Eng. Part A 15 (2008) 913–921.
[27] R. Srikar, A.L. Yarin, C. Megaridis, A. Bazilevsky, E. Kelley, Desorption-limited mechanism of release from polymer nanofibers, Langmuir 24 (2008) 965–974.
[28] M. Gandhi, R. Srikar, A.L. Yarin, C.M. Megaridis, R.A. Gemeinhart, Mechanistic examination of protein release from polymer nanofibers, Mol. Pharmaceutics 6 (2009) 641–647.
[29] S. Zupancic, S. Sinha-Ray, S. Sinha-Ray, J. Kristl, A.L. Yarin, Long-term sustained ciprofloxacin release from PMMA and hydrophilic polymer blended nanofibers, Mol. Pharmaceutics 13 (2015) 295–305.
[30] R. Sridhar, R. Lakshminarayanan, K. Madhaiyan, V.A. Barathi, K.H.C. Lim, S. Ramakrishna, Electrosprayed nanoparticles and electrospun nanofibers based on natural materials: applications in tissue regeneration, drug delivery and pharmaceuticals, Chem. Soc. Rev. 44 (2015) 790–814.
[31] S.P. Zupancic, S. Sinha-Ray, S. Sinha-Ray, J. Kristl, A.L. Yarin, Controlled release of ciprofloxacin from core–shell nanofibers with monolithic or blended core, Mol. Pharmaceutics 13 (2016) 1393–1404.
[32] J.H. Park, P.V. Braun, Coaxial electrospinning of self-healing coatings, Adv. Mater. 22 (2010) 496–499.
[33] S. Sinha-Ray, D. Pelot, Z. Zhou, A. Rahman, X.-F. Wu, A.L. Yarin, Encapsulation of self-healing materials by coelectrospinning, emulsion electrospinning, solution blowing and intercalation, J. Mater. Chem. 22 (2012) 9138–9146.
[34] X.F. Wu, A. Rahman, Z. Zhou, D.D. Pelot, S. Sinha-Ray, B. Chen, S. Payne, A.L. Yarin, Electrospinning core-shell nanofibers for interfacial toughening and self-healing of carbon-fiber/epoxy composites, J. Appl. Polym. Sci. 129 (2013) 1383–1393.
[35] X.F. Wu, A.L. Yarin, Recent progress in interfacial toughening and damage self-healing of polymer composites based on electrospun and solution-blown nanofibers: an overview, J. Appl. Polym. Sci. 130 (2013) 2225–2237.
[36] M.W. Lee, S. An, C. Lee, M. Liou, A.L. Yarin, S.S. Yoon, Self-healing transparent core–shell nanofiber coatings for anti-corrosive protection, J. Mater. Chem. A 2 (2014) 7045–7053.
[37] M.W. Lee, S. An, C. Lee, M. Liou, A.L. Yarin, S.S. Yoon, Hybrid self-healing matrix using core-shell nanofibers and capsuleless microdroplets, ACS Appl. Mater. Interfaces 6 (2014) 10461–10468.
[38] M.W. Lee, S. An, H.S. Jo, S.S. Yoon, A.L. Yarin, Self-healing nanofiber-reinforced polymer composites. 1. Tensile testing and recovery of mechanical properties, ACS Appl. Mater. Interfaces 7 (2015) 19546–19554.
[39] M.W. Lee, S. An, H.S. Jo, S.S. Yoon, A.L. Yarin, Self-healing nanofiber-reinforced polymer composites. 2. Delamination/debonding and adhesive and cohesive properties, ACS Appl. Mater. Interfaces 7 (2015) 19555–19561.
[40] S. An, M. Liou, K.Y. Song, H.S. Jo, M.W. Lee, S.S. Al-Deyab, A.L. Yarin, S.S. Yoon, Highly flexible transparent self-healing composite based on electrospun core–shell nanofibers produced by coaxial electrospinning for anti-corrosion and electrical insulation, Nanoscale 7 (2015) 17778–17785.
[41] M.W. Lee, S.S. Yoon, A.L. Yarin, Solution-blown core-shell self-healing nano- and microfibers, ACS Appl. Mater. Interfaces 8 (2016) 4955–4962.
[42] M.W. Lee, S. Sett, S.S. Yoon, A.L. Yarin, Fatigue of self-healing nanofiber-based composites: static test and subcritical crack propagation, ACS Appl. Mater. Interfaces 8 (2016) 18462–18470.
[43] M.W. Lee, S. Sett, S.S. Yoon, A.L. Yarin, Self-healing of nanofiber-based composites in the course of stretching, Polymer 103 (2016) 180–188.
[44] A.L. Yarin, S. Sinha-Ray, B. Pourdeyhimi, Meltblowing: multiple polymer jets and fiber-size distribution and lay-down patterns, Polymer 52 (2011) 2929–2938.
[45] X. Zhuang, X. Yang, L. Shi, B. Cheng, K. Guan, W. Kang, Solution blowing of submicron-scale cellulose fibers, Carbohydr. Polym. 90 (2012) 982–987.
[46] B. Vazquez, H. Vasquez, K. Lozano, Preparation and characterization of polyvinylidene fluoride nanofibrous membranes by forcespinning™, Polym. Eng. Sci. 52 (2012) 2260–2265.
[47] R. Ma, J. Lee, D. Choi, H. Moon, S. Baik, Knitted fabrics made from highly conductive stretchable fibers, Nano Lett. 14 (2014) 1944–1951.
[48] S. Sinha-Ray, M.W. Lee, S. Sinha-Ray, S. An, B. Pourdeyhimi, S.S. Yoon, A.L. Yarin, Supersonic nanoblowing: a new ultra-stiff phase of nylon 6 in 20–50 nm confinement, J. Mater. Chem. C 1 (2013) 3491–3498.
[49] L. Persano, A. Camposeo, C. Tekmen, D. Pisignano, Industrial upscaling of electrospinning and applications of polymer nanofibers: a review, Macromol. Mater. Eng. 298 (2013) 504–520.
[50] S. An, M.W. Lee, H.S. Jo, S.S. Al-Deyab, S.S. Yoon, Weaving nanofibers by altering counter-electrode electrostatic signals, J. Aerosol Sci. 95 (2016) 67–72.
[51] Y. Si, X. Mao, H. Zheng, J. Yu, B. Ding, Silica nanofibrous membranes with ultra-softness and enhanced tensile strength for thermal insulation, RSC Adv. 5 (2015) 6027–6032.
[52] Y. Zhang, A.L. Yarin, Carbon nanofibers decorated with poly(furfuryl alcohol)-derived carbon nanoparticles and tetraethylorthosilicate-derived silica nanoparticles, Langmuir 27 (2011) 14627–14631.
[53] S. An, H.S. Jo, D.Y. Kim, H.J. Lee, B.K. Ju, S.S. Al-Deyab, J.H. Ahn, Y. Qin, M.T. Swihart, A.L. Yarin, S.S. Yoon, Self-junctioned copper nanofiber transparent flexible conducting film via electrospinning and electroplating, Adv. Mater. 28 (2016) 7149–7154.
[54] J. Yu, J. Xiong, B. Cheng, S. Liu, Fabrication and characterization of Ag–TiO_2 multiphase nanocomposite thin films with enhanced photocatalytic activity, Appl. Catal., B 60 (2005) 211–221.
[55] G. Colon, M. Maicu, M.S. Hidalgo, J. Navio, Cu-doped TiO_2 systems with improved photocatalytic activity, Appl. Catal. B 67 (2006) 41–51.
[56] B. Yuan, Y. Pan, Y. Li, B. Yin, H. Jiang, A highly active heterogeneous palladium catalyst for the Suzuki-Miyaura and Ullmann coupling reactions of aryl chlorides in aqueous media, Angew. Chem. 122 (2010) 4148–4152.
[57] S. Wittmann, A. Schätz, R.N. Grass, W.J. Stark, O. Reiser, A recyclable nanoparticle-supported palladium catalyst for the hydroxycarbonylation of aryl halides in water, Angew. Chem. Int. Ed. 49 (2010) 1867–1870.
[58] S. Bae, H. Kim, Y. Lee, X. Xu, J.-S. Park, Y. Zheng, J. Balakrishnan, T. Lei, H.R. Kim, Y.I. Song, Roll-to-roll production of 30-inch graphene films for transparent electrodes, Nat. Nanotechnol. 5 (2010) 574–578.
[59] D.S. Hecht, L. Hu, G. Irvin, Emerging transparent electrodes based on thin films of carbon nanotubes, graphene, and metallic nanostructures, Adv. Mater. 23 (2011) 1482–1513.
[60] L. Li, Z. Yu, W. Hu, C.H. Chang, Q. Chen, Q. Pei, Efficient flexible phosphorescent polymer light-emitting diodes based on silver nanowire-polymer composite electrode, Adv. Mater. 23 (2011) 5563–5567.
[61] S. Wei, J. Shi, H. Ren, J. Li, Z. Shao, Fabrication of Ag/Cu_2O composite films with a facile method and their photocatalytic activity, J. Mol. Catal. A: Chem. 378 (2013) 109–114.
[62] L. Zhang, X. Wang, Photocatalytic performance of Cu_2O and Ag/Cu_2O composite octahedra prepared by a propanetriol-reduced process, Appl. Phys. A 117 (2014) 2189–2196.
[63] S. Gao, Z. Li, K. Jiang, H. Zeng, L. Li, X. Fang, X. Jia, Y. Chen, Biomolecule-assisted in situ route toward 3D superhydrophilic Ag/CuO micro/nanostructures with excellent artificial sunlight self-cleaning performance, J. Mater. Chem. 21 (2011) 7281–7288.
[64] H. Katsumata, Y. Oda, S. Kaneco, T. Suzuki, Photocatalytic activity of Ag/CuO/WO_3 under visible-light irradiation, RSC Adv. 3 (2013) 5028–5035.
[65] X. Liu, Z. Li, C. Zhao, W. Zhao, J. Yang, Y. Wang, F. Li, Facile synthesis of core–shell CuO/Ag nanowires with enhanced photocatalytic and enhancement in photocurrent, J. Colloid Interface Sci. 419 (2014) 9–16.
[66] X. Zhang, L. Wang, C. Liu, Y. Ding, S. Zhang, Y. Zeng, Y. Liu, S. Luo, A Bamboo-inspired hierarchical nanoarchitecture of Ag/CuO/TiO_2 nanotube array for highly photocatalytic degradation of 2, 4-dinitrophenol, J. Hazard. Mater. 313 (2016) 244–252.
[67] D.R. Lide, Handbook of Chemistry and Physics, CRC Press, 2004.